Emirates Journal for Engineering Research

Volume 29 | Issue 1 Article 1

11-18-2023

Steady and Transient Study of Conjugate Heat Transfer in Regenerative Cooled Nozzle

khaled bensayah
University of Laghouat/Algeria & INSA of Rouen/France, k.bensayah@lagh-univ.dz

khadidja Kamri
University of Laghouat/Algeria, kha.kamri@yahoo.com

Steady And Transient Study Of Conjugate Heat Transfer In Regenerative Cooled Nozzle

Abstract: The Heat transfer is one of the most serious challenges that exist in a supersonic nozzle flow. The combustion chamber wall and the nozzle are exposed to high-temperature gases during combustion and gas expansion, which can eventually lead to structural failure. This paper reports a computational study of steady and transient conjugate heat transfer in regenerative water cooled nozzle. Numerical computation solved Reynolds-averaged equations based on RSM-Omega turbulence model coupling with solid-phase heat conduction equation and with coolant-phase. The effect of four inlet cooled approach length 0 inch, 6 inch, 12 inch and 18 inch are studied and validated against the experiments available data. The gas-side wall temperature is also provided by numerical simulations, which show excellent agreement with experimental data. It is concluded that cooling the entire inlet-length is required when using high combustion gases and that when using moderate temperatures, the longer cooled length gives a lower maximum temperature located just upstream of the nozzle throat. Contours of temperature of transient study are presented for 5.18 bar and 10 bar inlet gas stagnation pressure and for different coolant mass flow rate. This study analyse in detail the effect of heating on the skin friction coefficient and wall heat transfer. A qualitative effect of wall cooling was obtained from the calculated values of the thickness of displacement, of momentum and of energy was presented.

Keywords: Transient simulation, Conjugate heat transfer, Compressible flow, Regenerative nozzle cooling, High temperature flows, RSM-Omega turbulence model, Shear flow correction

1. INTRODUCTION

The nozzle, as an energy conversion and thrust force producing device for the rocket, converts the thermal energy of the gases into kinetic energy. Hot gases flow at high speeds inside the nozzle, with gas temperatures exceeding 3500 K in most cases. The heat transfer between the hot gases and the nozzle via convection and radiation raises the nozzle temperature to 2500K. Working at high temperatures continuously poses a significant challenge to the nozzle's

safety and reliability [1,2]. Thermal fatigue, material failure, or surface ablation [3,4] may result from the resulting thermal constraints on the nozzle wall. Although no general theory of acceptable fatigue or ablation process of heterogeneous materials exists, it has been demonstrated to be generally related to heat transfer.

The necessity for a detailed understanding of heat transfer associated with turbulent boundary layer in supersonic flows develops as a result of the tendency to utilize large-expansion-area nozzles to enhance propulsive performance [5-8]. Depending on the wall's design, the added weight of the wall offsets the performance benefit of a yet higher area ratio for specific nozzle aspect ratios. Calculating friction losses is therefore essential to determining real performance [9]. Knowledge of the boundary layer is required by other recent advancements, such as shock production for thrust vector control [10–12].

Furthermore, accurate accounting of cooling requirements for hot-gas-exposed nozzles necessitates the prediction of local heat-transfer coefficients [13-18]. All of the prediction techniques failed to produce consistent agreement with the experimental boundary layer peak heat transfer coefficients. The experimental results showed that the 1/7-power law for a turbulent boundary layer and its associated temperature did not describe the thermal boundary layer in the nozzle's supersonic region [24].

The majority of conventional analyses of turbulent boundary layers in accelerated supersonic flows rely on empirical data from studies with near-zero acceleration. However, various analyses produce widely disparate predictions of turbulent boundary layer development in supersonic flows, particularly when heat transfer is involved.

According to the findings of Boldman et al., [19], extreme changes in velocity boundary layer thickness at the nozzle inlet resulted in a minor difference in throat heat transfer. In contrast, various throat heat transfer rates are caused by changes in the thickness of the thermal boundary layer at the nozzle entrance. A differential analysis was developed in order to provide a simple prediction of heat transfer. This method failed at the nozzle's subsonic region and necessitates the calculation of the entire nozzle boundary-layer at the exit nozzle point. When the momentum thickness Reynolds number is replaced by the energy thickness Reynolds number in the momentum heat analogy (Bartz theory [20-22]), the turbulent integral boundary-layer theory is one of the most commonly used methods for predicting heat transfer in nozzle flows; this method provides reasonably accurate predictions of heat transfer.

Internal and external heat transfer predictions, metal temperature distribution, wall cooling methods, and ceramic coatings are all important research areas in rocket nozzle heat transfer.

Internal convection is a complex phenomenon that depends on flow velocity and gas temperature, and there is significant uncertainty associated to both numerical predictions and experimental measurements.

There is a high demand for accurate numerical tools for determining temperatures on the nozzle surface and throughout the entire solid body of the nozzle within precision limits. Small errors in determining the temperature distribution can have a significant impact on the evaluation of the nozzle life. It is extremely difficult to find enough data in relevant literature to compare experimental or numerical results for the problem under consideration in this study.

In this study, we examined the experiment of Back et al., [23], who used a combustion chamber in which compressed air is heated by internal methanol combustion and mixed to become homogeneous before entering the nozzle. The nozzle had a throat diameter of 1.803 inches, a contraction area ratio of 7.75 to 1, an expansion area ratio of 2.68 to 1, for a convergent-divergent nozzle of 30°-15°. After the validation of the model in predicting the conjugate heat transfer, the present study focuses on the cooled-length effect on the heat transfer rate.

Heat transfer data were obtained using thermocouples implanted in plugs pressed into the wall of the water-cooled nozzle to measure steady-state temperatures. The nozzle was fabricated from type 502 stainless steel with a wall thickness of approximately 0.292 inches. We approached the simulation with co-current water cooling in the direction of flow, using numerically optimized flow rates, as the cooling system is completely absent in this study, including the mass flow rate and pressure of the water.

Thermal conductivity of the material can be estimated using Back et al., [24] temperature gradient and thermal flux. It is compared to other data that gives a variable thermal conductivity with temperature according to the formula $\lambda = A + BT$, the density of the material, the specific heat at constant pressure, and the thermal conductivity are given by $\rho = 7753$ kg/m3; $c_p = 486$ J/kg.K and $\lambda = 38.39 - 0.0061 \cdot T$ W/m.K, respectively.

2. Governing equations and turbulence modelling

The RSM $-\omega$ is a powerful model because, among other things, it has the ability to better simulate stagnation flow, reattachment, and curvature effects due to the accuracy of the production terms and the ability to better reflect the flow history. Advances in Reynolds Stress modeling are being made continuously. This model [25-27] solves a transport equation and a dissipation rate equation for each term of the Reynolds stress tensor.

The system of equations governed the turbulent compressible gas may be written as

$$\frac{\partial \bar{\rho}}{\partial t} + \frac{\partial}{\partial x_j}\left(\bar{\rho}\widetilde{U_j}\right) = 0 \quad (1)$$

$$\frac{\partial \bar{\rho}\widetilde{U_i}}{\partial t} + \frac{\partial}{\partial x_j}\left(\bar{\rho}\widetilde{U_i}\widetilde{U_j} + \bar{\rho}\widetilde{u_i''u_j''}\right) = \frac{\partial \overline{\sigma_{ij}}}{\partial x_j} - \frac{\partial \bar{P}}{\partial x_i} \quad (2)$$

$$\frac{\partial \bar{\rho}\tilde{E}_t}{\partial t} + \frac{\partial \tilde{U}_j(\bar{\rho}\tilde{E}_t+\bar{P})}{\partial x_j} = \frac{\partial}{\partial x_j}\left(\overline{\sigma_{ij}U_i} - \bar{\rho}\widetilde{u_i''u_j''}\tilde{U}_i - \frac{1}{2}\bar{\rho}\widetilde{u_i''u_i''u_j''}\right) - \frac{\partial}{\partial x_j}\left(\bar{\rho}\gamma c_v\overline{T''u_j''} - \overline{k_c\frac{\partial T}{\partial x_j}}\right) \quad (3)$$

Where $\bar{\rho}$, $\tilde{U}_j$, $\bar{P}$ and $\tilde{E}_t$ are the density, velocity and the pressure and the total energy respectively.

$$\bar{\rho}R_{ij} = -\overline{\rho u_i''u_j''} \quad (4)$$

$$\frac{\partial \bar{\rho}R_{ij}}{\partial t} + \frac{\partial(\bar{\rho}U_kR_{ij})}{\partial x_k} = P_{ij} + \Pi_{ij} - \tfrac{2}{3}\beta^* f_{\beta^*}\bar{\rho}\omega k\delta_{ij} + \frac{\partial}{\partial x_k}\left[\left(\mu + \frac{\mu_t}{\sigma_k}\right)\frac{\partial R_{ij}}{\partial x_k}\right] \quad (5)$$

$$\frac{\partial \bar{\rho}\omega}{\partial t} + \frac{\partial(\bar{\rho}U_k\omega)}{\partial x_k} = \frac{\alpha\bar{\rho}\omega}{k}R_{ij}\frac{\partial U_i}{\partial x_j} - \bar{\rho}\beta f_\beta\omega^2 + \frac{\partial}{\partial x_k}\left[\left(\mu + \frac{\mu_t}{\sigma_\omega}\right)\frac{\partial \omega}{\partial x_k}\right] + \sigma_d\frac{\bar{\rho}}{\omega}\frac{\partial k}{\partial x_j}\frac{\partial \omega}{\partial x_j} \quad (6)$$

The pressure-strain correlation is given by

$$\Pi_{ij} = \beta^* f_{\beta^*}C_1\bar{\rho}\omega\left(R_{ij} + \frac{2}{3}k\delta_{ij}\right) - \hat{\alpha}\left(P_{ij} - \frac{2}{3}P\delta_{ij}\right) - \hat{\beta}\left(D_{ij} - \frac{2}{3}P\delta_{ij}\right) - \hat{\gamma}\bar{\rho}k\left(S_{ij} - \frac{1}{3}S_{kk}\delta_{ij}\right) \quad (7)$$

The production tensor of Reynolds stresses is given by:

$$P_{ij} = -\overline{\rho u_i''u_k''}\frac{\partial U_j}{\partial x_k} - \overline{\rho u_j''u_k''}\frac{\partial U_i}{\partial x_k} \quad (8)$$

With $k = -R_{ii}/2$, $\mu_t = \bar{\rho}k/\omega$ and $P = P_{kk}/2$

The tensor D_{ij} differs in the dot-product indices from the production tensor

$$D_{ij} = -\overline{\rho u_i''u_k''}\frac{\partial U_k}{\partial x_j} - \overline{\rho u_j''u_k''}\frac{\partial U_k}{\partial x_i} \quad (9)$$

The closure coefficients of the model are:

$\hat{\alpha} = (8 + C_2)/11$, $\hat{\beta} = (8C_2 - 2)/11$, $\hat{\gamma} = (60C_2 - 4/55$, $C_1 = 9/5, C_2 = 10/19$, $\alpha = 13/25$, $\beta = \beta_0 f_\beta$, $\beta^* = 9/100$, $\sigma_k = 2$, $\sigma = 5/3$, $\beta_0 = 0.0708$, $\sigma_d = 0$ for $(\partial k/\partial x_j \cdot \partial\omega/\partial x_j) \le 0$, $\sigma_d = 1/8$ for $(\partial k/\partial x_j . \partial\omega/\partial x_j) > 0$, $f_\beta = (1 + 70X_\omega)/(1 + 80X_\omega)$, $X_\omega = \left|W_{ij}W_{jk}\hat{S}_{ki}/(\beta^*\omega)^3\right|$, $\hat{S}_{ki} = S_{ki} - 0.5(\partial\hat{u}_m/\partial x_m)\delta_{ki}$, $S_{ij} = 0.5(\partial U_i/\partial x_j + \partial U_j/\partial x_i)$, $W_{ij} = 0.5(\partial U_i/\partial x_j - \partial U_j/\partial x_i)$, $f_\beta^* = 1$ if $x_k \le 0$ & $f_\beta^* = (1 + 640x_k^2)/(1 + 400x_k^2)$ if $x_k > 0$.

If the case with non-Shear-Flow-Corrections f_{β^*} and f_β will be set equal to 1.

3. NUMERICAL METHOD

A parallel finite volume discretization based on full Favre averaging Navier-Stokes unsteady equations is used to solve axisymmetric flows using RSM-Omega turbulence model.

The simulations were processed using Ansys Fluent CFD software. The discretization used the second-order upwind scheme with double precision accuracy for convective terms, second-order method is adopted for pressure term. In the fluid zones, the steady, times-averaged Navier-Stokes equations were solved, and pressure-velocity coupling was achieved using a SIMPLE

pressure correction algorithm. In the solid zone, only the Fourier equation for heat diffusion was solved.

At the fluid-solid interfaces, an energy balance was satisfied at each iteration, such that the heat flux at the wall on the fluid side was equal in magnitude and opposite in sign to the heat flux on the solid side. The temperature of the boundary itself was adjusted during each iteration to meet this condition. The solutions are converged to normalized residual mean square (RMS) of the order of 10^{-5} or lower. Barbosa et al,. [4] concluded that this unified approach can be fully applied to simulate conjugate heat transfer. The major difference between our study and [4], is that in our study, the boundary layer is fully solved using the RSM-Omega turbulence model for both steady state and transient study, the distance between the wall and first point is 10^{-7}m, which gives y^+ lower than 0.2.

For the unsteady calculations, the time step size used is $5x10^{-5}$ second, and to reach reasonable unsteady solution at each time step, 50 iterations per time step was used. A second order implicit scheme is used for time discretization.

The technique used in this study, especially for transient computation, is designed to prevent nozzle material damage and to ensure that the cooling process is progressing well. In fact, if we begin the nozzle with hot gases and the cooling at the same time, the nozzle's gases will develop quickly and the heat transfer through the walls will occur immediately, while the cooler takes its time to begin cooling this wall, and in this case, the wall may reach an undesirable temperature.

This process is typically the most popular, especially in space applications where the liquid hydrogen starts to cool the nozzle before the combustion gases are fired. In this case, the nozzle is started with the desired generating pressure and a moderate temperature of about 400 K, assuming that the gas is not heated by the combustion products. Meanwhile, the cooler is launched appropriately to reach a steady state of cooling.

The coolant is brought to a quasi-stationary state before the gas temperature is raised to the required level.

4. RESULTS AND DISCUSSIONS

The geometry of the JPL (Jet Propulsion Laboratory) nozzle was created using a matlab program, grid resolution and the boundary conditions used for the analysis are shown in Figure 1.

The grid independence study was accorded a considerable importance, because the turbulence model used need to resolve the entirely boundary layer. Using a variety of meshes, including coarse meshes with 30000 cells, medium meshes with 70000 cells, and fine meshes with 111000 cells, the sensitivity of the grid on the numerical predictions has been examined.

The predictions for different grids are identical for a mesh size above 70000 cells. The fine grid has been adopted in this computations, the detail of the fine mesh is presented in table 1. The laminar viscous sublayer had to be

resolved; this has been achieved by keeping the maximum non-dimensional wall distance (y^+) of the first point near the wall less than 0.25, which is sufficiently smaller than 1 (see Figure 2). The first point distance to the wall is 10-7 m in the gas side wall and 2x10-6 m in the coolant side wall.

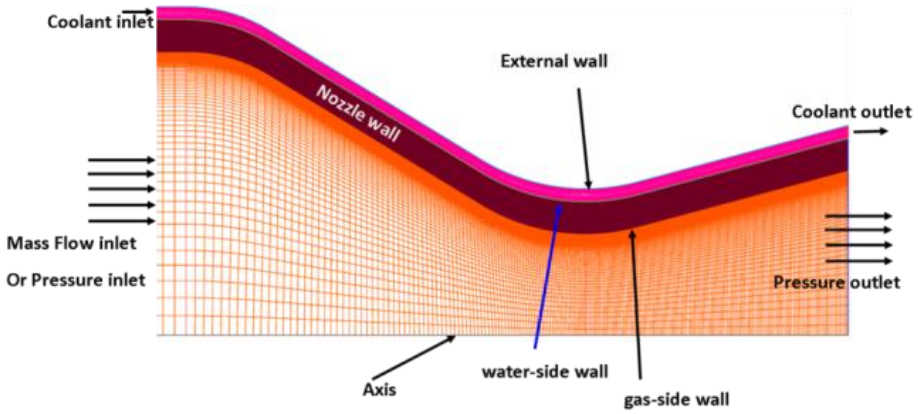

Figure 1 - JPL nozzle geometry, mesh and boundary conditions

Table 1. Grid resolution

section	inlet cooled section	Convergent section	Divergent section
Nozzle	120 ×150	100 ×150	150 ×150
wall	120 ×70	100 ×70	150 ×70
coulant	120 ×80	100 ×80	150 ×80

The assumption of a calorically perfect gas is not valid [28-30]. Therefore, fluid properties, such as the specific heat, thermal conductivity, and viscosity, are considered to vary with temperature.

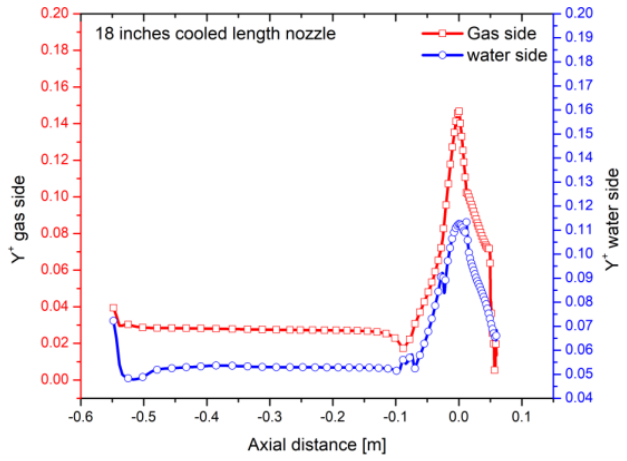

Figure 2 - y^+ variation along the gas side wall nozzle and water side

In general, the fluid properties have been defined as polynomial functions of temperature, the viscosity of air vary according to the known Sutherland law. Property values of air were obtained from the National Aeronautics and Space Administration (NASA) online program CEARUN [31].

The water inlet pressure was 10 atm for all simulations. The thermos-physical properties of the density, specific heat, thermal conductivity and viscosity are taken from the NIST (National Institute of Standards and Technology) data. NIST assumes thermodynamic equilibrium at the coolant pressure and consequently has a discontinuity of enthalpy vs temperature during the liquid-vapor phase change.

Significant variances in gas expansion are seen, resulting in dramatic changes in flow characteristics between variable and constant fluid properties. The assumption of constant fluid properties becomes problematic in many compressible flow situations with high combustion gas temperature, and a variable fluid property analysis appears to be more appropriate.

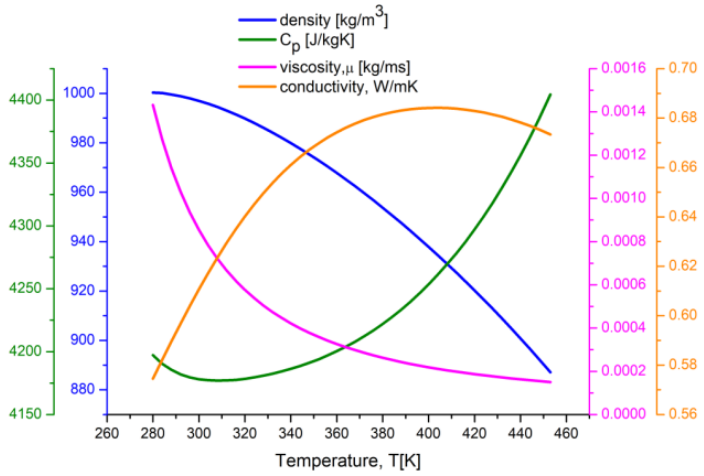

Figure 3 - water properties variation with temperature for 10 bar pressure

4.1 Validation of results

To validate of the numerical solver and assess the turbulence model, we compared the numerical results to the available experimental data of back et al., [23].

Four cases are studied, the first case, called 0 inch, in this case the length of the cooled inlet is equal to zero, i.e that the nozzle is cooled from its originate inlet (see Figure 4). This case takes the name TEST 315 in the experimental data of Back et al., [23]. The operating conditions were set at P_0 =74.6 psia (5.1434 bar) of stagnation pressure and T_0=1516 °R (842.22 K) for stagnation temperature, the gas (heated Air) was treated as thermally perfect gas, property vary with temperature. The ratio of specific heats γ vary with the

c_p. The coolant water enters with 10 bar of pressure, 300 K of temperature and the mass flow rate is 2kg/s. The Figure 5(a) shows the comparison between numerical simulation of the entire conjugate heat transfer and the experimental data of Back, in this figure the axial distribution of the gas-side nozzle wall is given. The numerical predictions are in excellent agreement with the experimental data; the error in the maximum throat temperature prediction is much smaller of about 0.3%, except for the nozzle inlet which the error is about 8%, this error is due to beginning of cooling in the case of 0 inch.
Figure 5b shows the axial evolution of wall temperature, density and wall pressure. The analysis of this figure shows that the density starts to increase and the temperature starts to decrease almost at the same position, which is 7 cm before the nozzle entrance, all this occurs at an almost constant chamber pressure of about 517410 [pa].

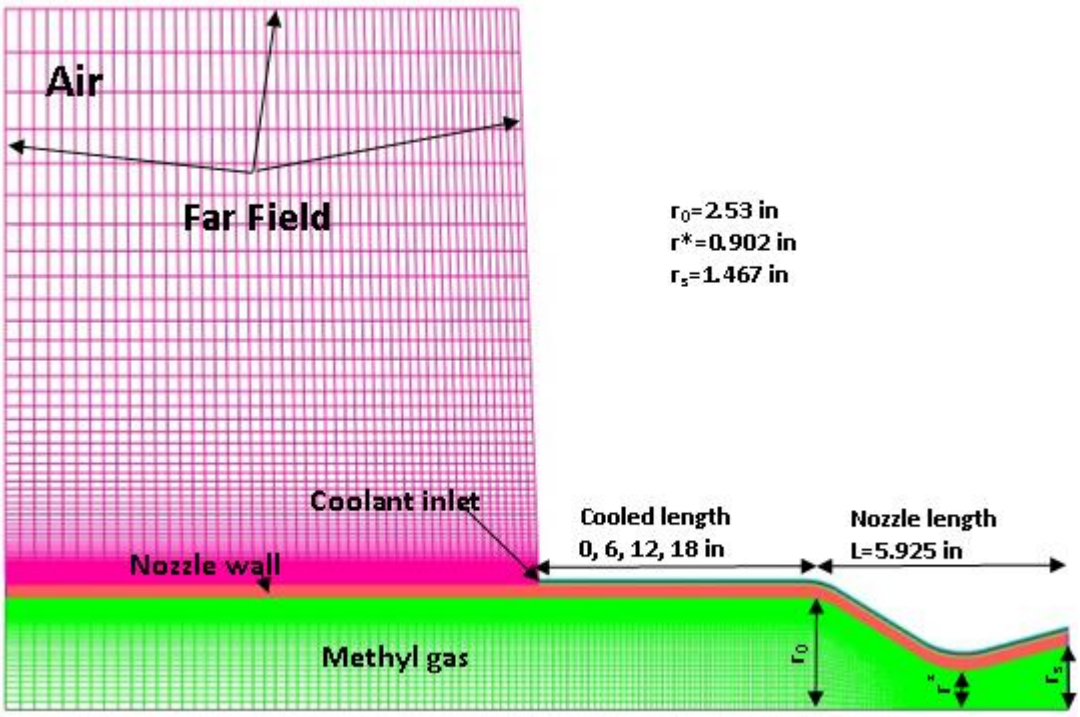

Figure 4 - Geometry and mesh of cooled length approach 0, 6, 12 or 18 inches (case of 6 inches)

This behavior continues in the same way, even when the flow enters the nozzle up to a distance of 1.4 cm, at this position the density reaches its maximum (5.32 kg/m^3) and the temperature reaches its minimum (373 K). After this distance the pressure starts to decrease with the density and consequently the temperature increases, this represents the conversion of the pressure energy into kinetic energy, the flow accelerate until the nozzle exit,

flow is considered isentropic with the absence of shocks. The temperature before the nozzle inlet continue to decrease to a minimum value of about 373 K, because the uncooled flow in the combustion chamber meets the cooled flow that starts just at the nozzle inlet, the temperature decreases and the density inevitably increases, because until this position the pressure is almost constant. Next the temperature increase to reach a maximum of about 480 K just upstream of the throat, in this case (0 inch) the exact position of the maximum heat is situated 4.9 mm upstream the geometric throat, this is the result of both maximum of mass flux at the edge of the boundary layer, $\rho_e u_e$ and the axial variation of the fluid properties and boundary-layer thickness parameters, it can be concluded that the wall temperature distributions and mass flow $\rho_e u_e$ distributions follow similar trends.

The maximum of friction coefficient at the throat can also be used to describe the highest temperature on the wall nozzle. In the divergent section immediately downstream of the throat, the temperature decreases with both decrease of density and pressure, axial distribution of wall friction velocity decrease dramatically with the increase of the area in the divergent section, all these parameters affect the wall temperature distribution.

The wall static-to-total pressure ratio (p_w/p_0) at the throat was always lower than the value based on one-dimensional isentropic flow ($p_w/p_0 = 0.5283$) as would be expected.

It should be noted here that the temperature of the surface of the combustion chamber is the same as that of the combustion gases, which means that it must be cooled or made of special materials, which is beyond our reach.

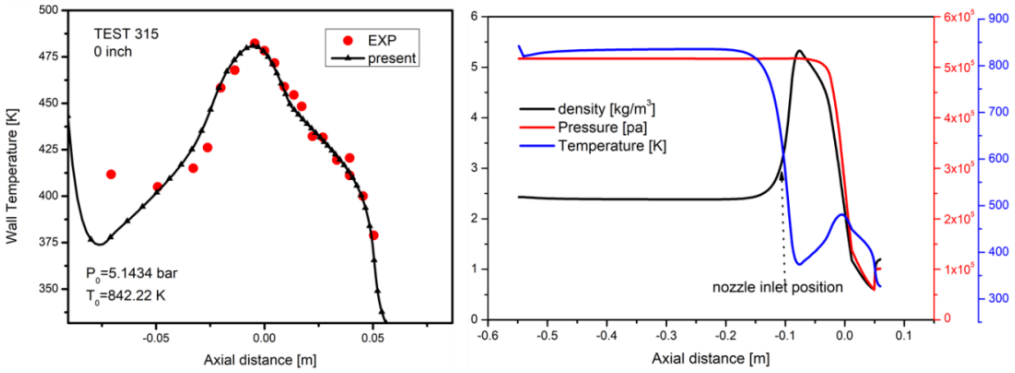

Figure 5 - (a) gas-side wall temperature comparison with experimental data [16] (b) Axial distribution of wall density, temperature and pressure for 0 inch case

The second case studied for the validation of the turbulence model and the conjugate heat transfer between the nozzle wall and the internal hot gas flow. The water mass flow rate is 2 kg/s, the coolant starts at a distance equal to 6 inches upstream the nozzle inlet. The temperature undergoes a sharp decrease

just at the meeting of the hot gas with the cooled flow at an axial position equal to 21.48 cm, which corresponds to the position of the beginning of cooling (6 inches before the nozzle inlet). From this position, the temperature remains almost constant at a plateau of about 373 K until the nozzle entrance. The flow is slightly accelerated, which reduces the temperature to a minimum of about 357 K, the corresponding pressure and density ratios are $p/p_0 = 0.997$ and $\rho/\rho_0 = 2.25$, respectively, where $p_0 = 518486$ pa and $\rho_0 = 2.24\ kg/m^3$ are stagnation conditions; this explains that the decrease in temperature corresponds to an increase in density at constant pressure.

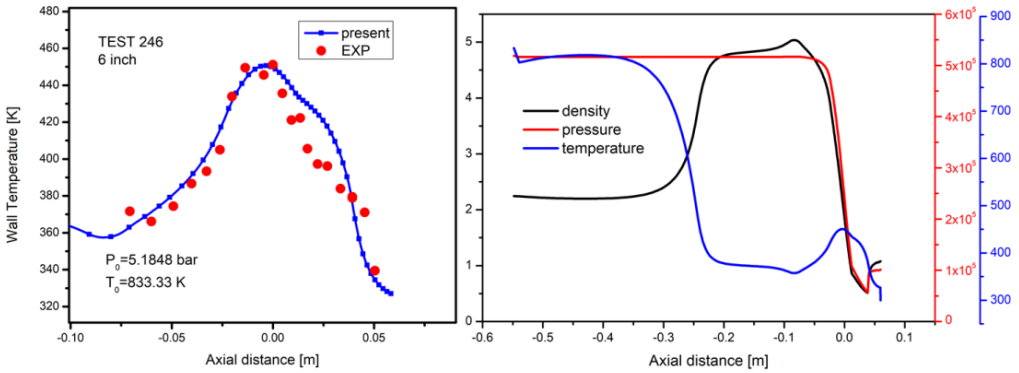

Figure 6 - (a) gas-side wall temperature comparison with experimental data [16] (b) Axial distribution of wall density, temperature and pressure for 6 inches cooled length case

In the convergent section and on the axis the flow expands, and the pressure, temperature and density decrease continuously with the acceleration of the flow. But on the wall, due to the increase in velocity friction, wall shear stress and mass flow rate, the temperature increases and reaches a maximum of about 450 K at a position 3.8 mm just upstream of the nozzle throat, the corresponding pressure and density ratios are $p/p_0 = 0.55$ and $\rho/\rho_0 = 0.98$, respectively. The numerical prediction agrees very well with the experimental data (Figure 6), the error in predicting the maximum gas side temperature is about 0.2%, and in the supersonic region the errors vary from 2% to 6%. All explanations and interpretations cited above of the phenomena encountered for the 0 inch case are valid for understanding of the physics of conjugate heat transfer for the other cases.

The anomaly encountered in this study is that one would expect cooling with a length of 18 inches to normally lead to a lower maximum temperature than that of 12 inches.

The maximum temperature for the 18-inch case is 462 K (Figure 8), while that of the 12-inch case is 443 K (Figure 7), which explains that the coolant mass flow rate and pressure are not the same for all cases measured by Back et al. [23]. According to the numerical investigations carried out during

the validation of the numerical calculations. For the same coolant pressure of 10 bar, the mass flow rate used to obtain the given experimental data for the 12-inch case is about 2.7 kg/s, while for the 18-inch case a mass flow rate of 1.5 kg/s is sufficient to get the same experimental results.

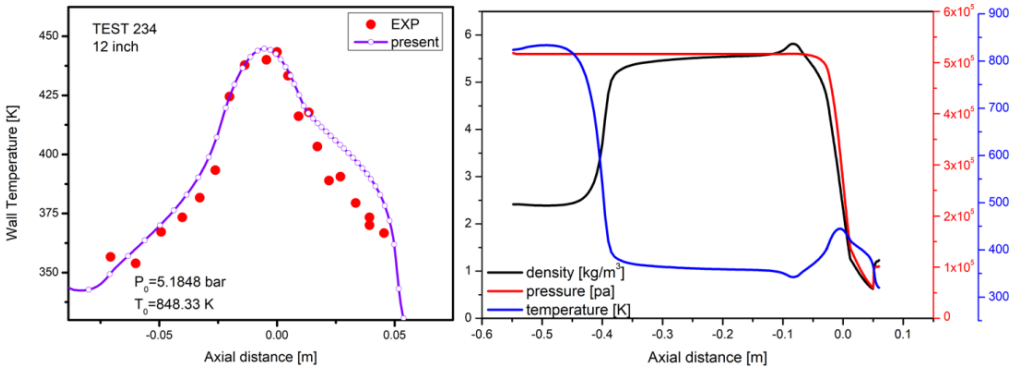

Figure 7 - (a) gas-side wall temperature comparison with experimental data [16] (b) Axial distribution of wall density, temperature and pressure for 12 inches cooled length case

It is difficult to judge the pertinence of the results obtained through validation to comprehend the effects of cooling length on the rate of heat transfer, and to make a meaningful comparison between all the cases studied, the same conditions should be used for the hot gases and the coolant.

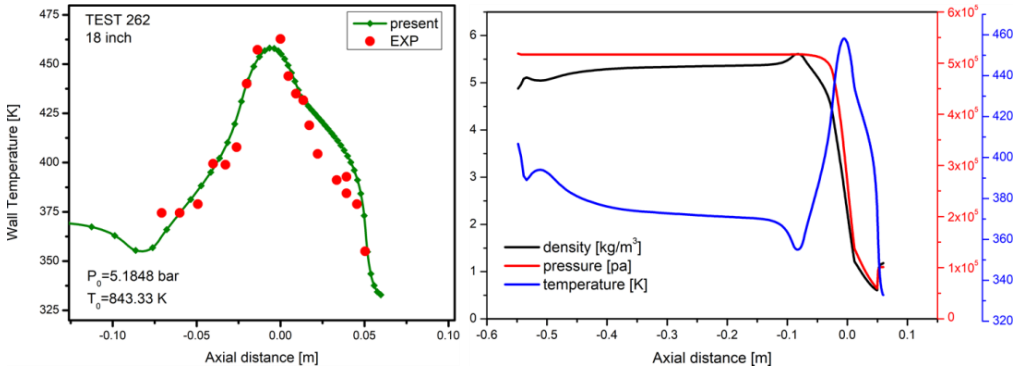

Figure 8 - (a) gas-side wall temperature comparison with experimental data [16] (b) Axial distribution of wall density, temperature and pressure for 18 inches cooled length case

To accomplish this comparison, we applied the same conditions for all cases, the pressure and stagnation temperature at the hot gas inlet are 9 bar and 1000 K, respectively. For the coolant the pressure is 10 bar and the mass flow is 2 kg/s.

The first interpretation of the comparison graph of Figure 9 between the four studied cases, clearly shows that the predictions can be separated into two

groups, one characterized by the uncooled combustion chamber (0 inch), and the others by the partially cooled combustion chamber (6, 12 inches), and the entirely cooled combustion chamber (18 inches). These findings show that the cooling of the combustion chamber is essential to protect its wall from high temperatures. Analysis of the results shows that with a cooling length equal to 18 inches, the maximum temperature localized on the nozzle throat decreases with a rate of 11% compared to the uncooled case.

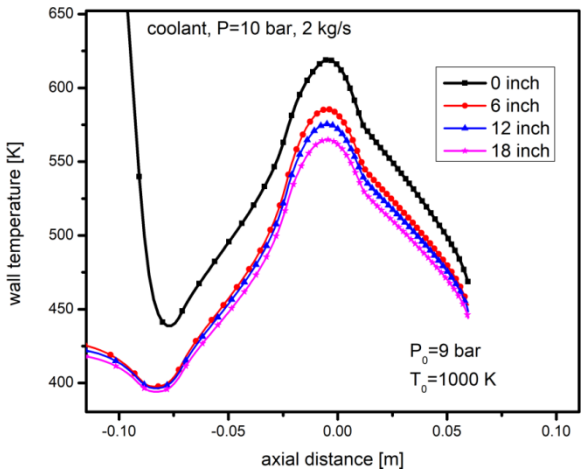

Figure 9 - Effect of cooled length inlet on the wall temperature

Figure 9 shows that as the cooling length increases, the combustion chamber temperature decreases, with the maximum temperature at the nozzle throat decreasing by 3% between the 18 inches and 12 inches cases, and by 6% between the 18 inches and 6 inches cases.
Thus, it is found that the 18 inches cooled-length quickly reduces the ratio of static-to-total temperature to a value of $T/T_0 = 0.43$. This shows that even when using real combustion temperatures of about 3500 K, the combustion chamber temperature reduces to a value of 1500 K, which is below the melting temperature of most metals, and this is only with the use of water cooling, whereas this temperature would be very low with cryogenic cooling, using liquid hydrogen or another efficient coolant.

4.2 Study of transient conjugate heat transfer

In order to study the effect of the variation of the generating pressure at the inlet of the nozzle, a comparison was made for the following two operating conditions, (P=10 bar, T=824.44 K) and (P=5.18bar, T=843.33K), the total temperature is a little shifted to reach the same experimental measurements of back et al. [23]. In fact, varying the inlet total pressure is to observe the effect resulting from a variation in the Reynolds number in the nozzle heat transfer. The coolant in these two simulations is water with mass flow rate (m=1.3769

kg/s), the water properties are taken variable with temperature, the pressure was about 1 bar and the temperature is equal to 300 k.

Figure 10 shows the transient temperature contour distributions on the wall nozzle, which indicates that the highest wall temperature of about (511.5 K and 453.5 K) on the hot gas-side respectively for pressure (10 bar and 5.18 bar) occurred at the position just upstream the throat region (x=-0.00489m). The pressure drop and temperature difference between the inlet and the throat region of the cooling channel are for the case (P=5.18bar, T=843.33K) and respectively for times equal to 5 s, 10 s and 15 s given by (4313 pa, 35.92 K) , (4278 pa, 43 K) and (4264 pa, 45 K); and given for the case with (P=10 bar, T=824.44 K) by (4251 pa, 51.8 K) , (4206 pa, 59.9 K) and (4186 pa, 61.56 K); the decrease in the pressure corresponds to the maximum speed reached in this region.

The wall temperature and heat transfer rate increased with increasing stagnation pressure due to larger mass flux. Increasing the pressure from 5.18 bar to 10 bar causes an increase in Reynolds number based on the diameter of the nozzle, its value is about 4.87×10^5 at the inlet of the nozzle and 1.19×10^6 at the throat position for P = 5.18 bar, and about 9.68×10^5 to 2.37×10^6 for the same positions for P = 10 bar. This increase leads to a nozzle wall heating, from which the maximum temperature has increased from 452 K for 5.18 bar to 510 K for 10 bar, this maximum is localized just upstream of the throat.

The skin friction coefficient ($C_f = 2\tau_w/\rho_e u_e^2$) and wall heat transfer q_w and many other parameters were affected. The effect of heating seems to reduce the coefficient of friction, regardless of the stream-wise location. The maximum of skin friction coefficient localized at the throat position decreased from 0.0051 to 0.0045, which corresponds to 14% of reduction without direct heating but an increase in wall temperature due to an increase in inlet pressure (the values of C_f is equal to 0.00272 and 0.00244 at 3 cm upstream the nozzle inlet, these values are in good agreement with those of Back et al., [23], who found 0.0026 and 0.0022 respectively). Because the wall shear stress ($\tau_w = \mu(\partial\tilde{u}/\partial y)_{y=0}$) increases with 70% for the same position from 811 pa to 1385 pa, this term which is directly proportional to C_f and therefore its rise typically increases the C_f , but there is also an increase by a factor of 1.98 in the density (ρ_e) evaluated at the edge of the boundary layer; we find that most of the differences in C_f observed as a result of heating are simply due to changes in fluid properties, but in a way not to ignore the variation in τ_w, and therefore in the profile of the velocity in the thin inner region close to wall, we notice that the Prandtl number is not equal to unity so that the physical extents of the velocity and temperature are not identical. These results were similar to the results of references [32] and Debiève et al. [33].

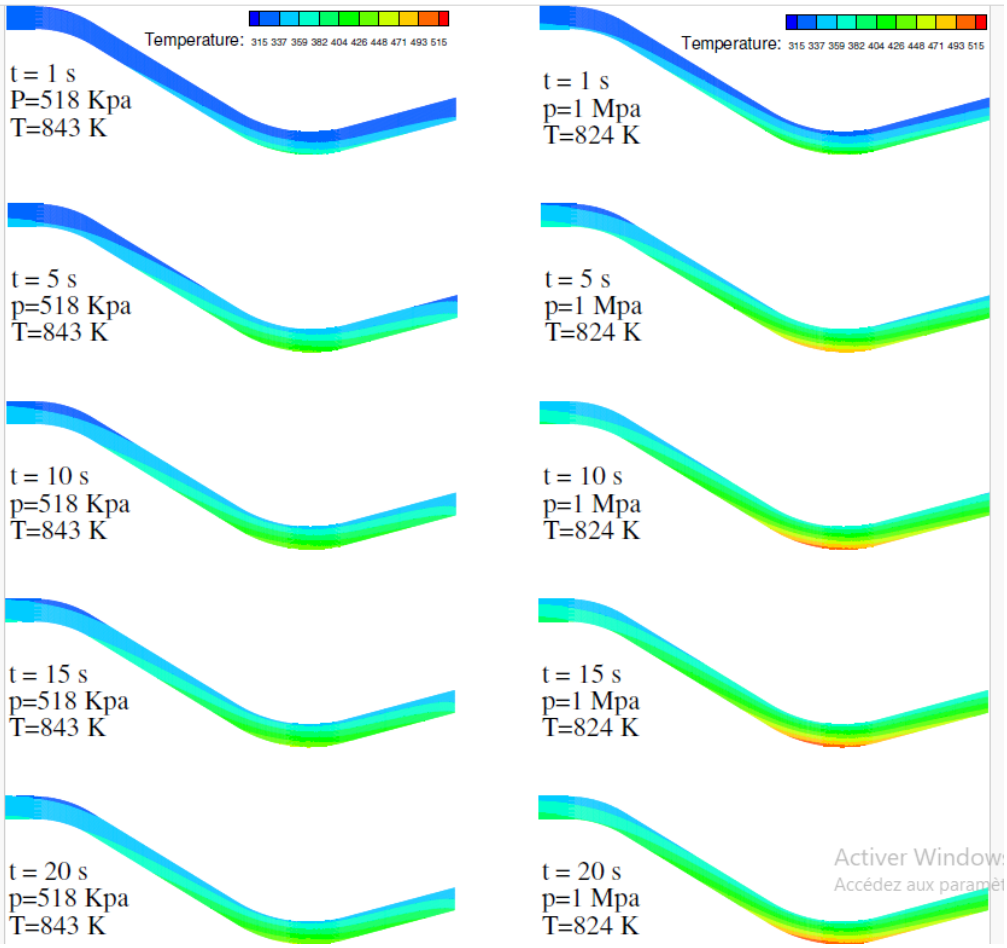

Figure 10 - transient temperature-contour in wall nozzle with different gas pressure, Pwater = 100 Kpa (1 bar) and mass flow rate 1.37 kg/s

An indication of the qualitative effects of increasing pressure and wall cooling, can be obtained from the calculated values of the thickness δ^*, θ and ϕ which presented the displacement, momentum and energy thickness respectively, given by the following equations:

$$\delta^*\left(1-\frac{\delta^*}{2R}\right)=\int_0^\infty\left(1-\frac{\rho u}{\rho_e U_e}\right)\left(1-\frac{y}{R}\right)dy \tag{10}$$

$$\theta\left(1-\frac{\theta}{2R}\right)=\int_0^\infty\frac{\rho u}{\rho_e U_e}\left(1-\frac{u}{U_e}\right)\left(1-\frac{y}{R}\right)dy \tag{11}$$

$$\phi\left(1-\frac{\phi}{2R}\right)=\int_0^\infty\frac{\rho u}{\rho_e U_e}\left(1-\left(\frac{T_0-T_w}{T_e-T_w}\right)\right)\left(1-\frac{y}{R}\right)dy \tag{12}$$

At the position 3 cm upstream the nozzle inlet, the boundary layer thicknesses δ^*, θ and ϕ are respectively 2.0718 mm, 2.087 mm and 0.726 mm for P=5.18 bar, Back et al. [16] have found respectively the results (1.4478 mm, 1.5494 mm and 0.7874 mm); and for P=10 bar we get 2.01 mm, 1.995 mm and 0.6562 mm. At the throat the thickness of the boundary layer becomes smaller, in fact it is difficult to accurately calculate this thickness, because the profile of the velocity is quite complicated, as close to the edge of the boundary layer the freestream velocity (u_e) exceeds its value on the axis, which is well explained by the negative values of displacement thickness (-0.1646 mm against the value -0.117 mm of Back et al. [16]), that means that the velocity profile could have a point of inflection within the flow without separation from the wall.

The effect of the mass flow rate of coolant has also been studied; the gas side wall and coolant side temperatures are represented by a contour in Figure 11, the mass flow rate is increased from 1.3769 kg/s to 13.769 kg/s while all other remain constant. The temperature decreases with increased coolant mass flux, the maximum gas-side wall temperature reduced from (511 K) to (478 K), the gas-side wall heat flux increases by a factor of 1.14 which occurs just upstream of the throat, and where the coolant velocity is high. The maximum coolant velocity and mass flux increase respectively from 2.628 m/s to 25.66 m/s near the throat, and from 2603 kg/m^{2}s to 25495 kg/m^{2}s with increased mass flow rate, the maximum skin friction coefficient ($C_f = 2\tau_w/\rho_e u_e^2$) located at the throat (minimum area), is very little influenced, increasing from 0.0045 to 0.00454 with increased mass flow rate.

The transient analysis shows that with the increase of coolant mass flow rate, the cooling process becomes more efficient, the comparison gives the following result; with the progress in time t = 1, 2, 3, 5 and 10 s respectively, the maximum gas-side ratio (T_w/T_0, for the case with m=1.3769 Kg/s) located at the throat was found equal respectively to 0.5315, 0.5606, 0.5788, 0.5995 and 0.6152; and for the case with m=13.769 kg/s, 0.5254, 0.5509, 0.5643, 0.5752 and 0.58.

For the water-side with m=1.3769 kg/s the ratio (T_w/T_{inlet}, T_{inlet}=300 K) is equal respectively to 1.0677, 1.0696, 1.1387, 1.1677 and 1.1935; and for m=13.769 kg/s it equal to 1.0161, 1.0275, 1.0329, 1.037 and 1.0394, which explain that the temperature of both gas-side and water-side (Figure 12) decrease very fast in time with the increase of coolant mass flux.

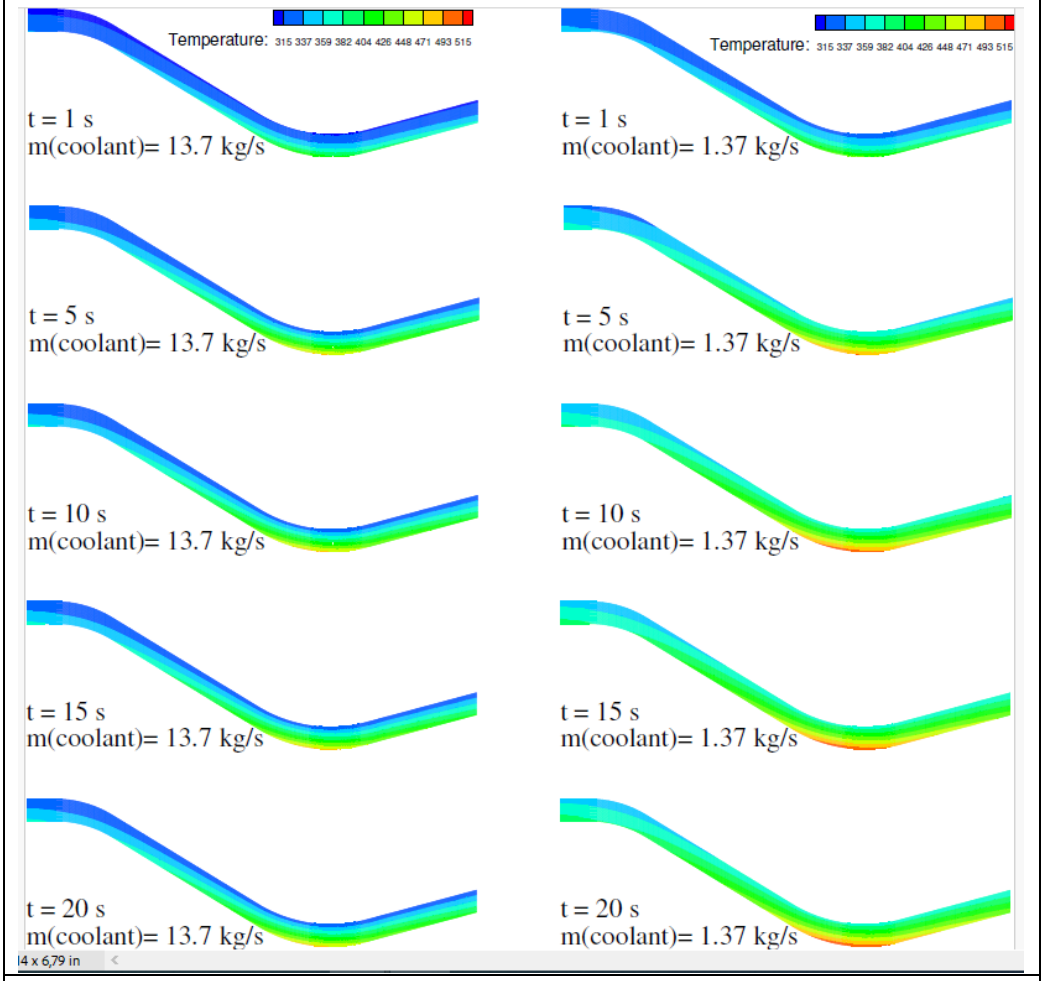

Figure 11 - transient temperature-contour with different coolant mass flow rate, and for P_0=10 bar and T_0=824 K for stagnation condition

It is noted here that the position of the maximum temperature of the water-side moves in time in downstream direction until the position just upstream of the throat. The maximum gas-side wall heat flux (just upstream of the throat) for (m=1.3769 kg/s) decreases with same progress in time and given respectively by 0.99, 0.90, 0.84, 0.78, 0.74 (MW/m^2) and for m=13.769 kg/s by 1.02, 0.92, 0.88, 0.85, 0.83 (MW/m^2), with the same trend, the wall heat flux decreases faster with the increase of coolant mass flux (see Figure 13). It can be seen that the maximum wall heat flux water-side increases with the increase of the coolant mass flux and increased in time, in these two cases the coolant water pressure was 1 bar, for the case with m = 1.3769 the maximum water temperature reached is of the order 372.69 K which just below the temperature of saturation (Tc = 372.76 K) then we cannot go more than T_0 = 985 K for the nozzle inlet gas temperature, the water evaporates and the cooling will have no sense, and the nozzle cannot survive.

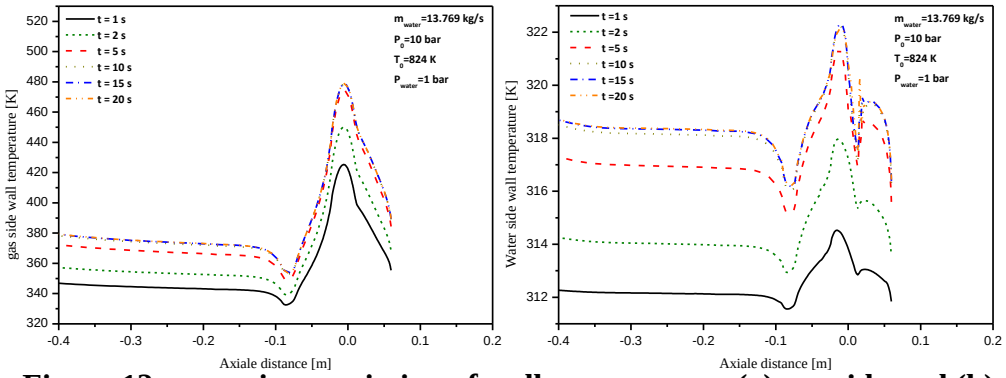

Figure 12 - transient variation of wall temperature, (a) gas side and (b) water side

With increased coolant mass flux to m=13.769 kg/s, the maximum supported temperature of the gas is more than 2100 K under the same conditions.

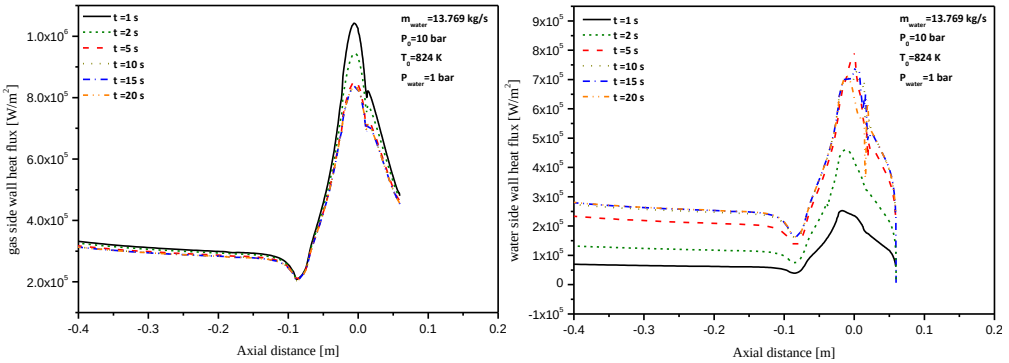

Figure 13 - transient variation of wall heat flux, (a) gas side and (b) water side

5. CONCLUSIONS

In this study, we conducted a comprehensive numerical investigation on the dynamic and thermal behavior of compressible flow and wall-fluid conjugate heat transfer within a water-cooled convergent-divergent nozzle. Our research focused on highlighting the crucial role of the cooled inlet length in the cooling process, which plays a vital role in maintaining the integrity of both the combustion chamber and the nozzle wall.

The numerical method employed for the study of fluid flow is the finite volume method, specifically utilizing a second-order Roe scheme. This numerical method is highly efficient and widely recognized for its

effectiveness in capturing discontinuities in the flow, particularly in the case of Reynolds-Averaged Navier-Stokes (RANS) turbulence.

To provide a summary of the research addressed in this study, the following conclusions can be drawn:

I- The RSM-Omega turbulence model, enhanced with the correction shear flow, demonstrated excellent agreement between the numerical predictions and experimental data.

II- The transient cooling study provided valuable insights into the cooling process strategy. It revealed that significant heat transfer occurs at the initial stage of cooling before reaching a stationary phase.

III- It is crucial and obligatory to initiate cooling before introducing hot gases into the nozzle, as the hot gases rapidly transition from the initial to the stationary state within 1-4 ms. The cooling time extends for approximately 40-60 s.

IV- All cases exhibited similar behavior in terms of gas-side wall temperature and wall heat flux, with peak values occurring slightly upstream from the throat.

V- Changes in the coolant-inlet length impact the distribution of the thermal boundary layer and subsequently affect the wall temperature distributions. The effect of the initial boundary-layer thickness on the gas-side wall temperature is more pronounced near the entrance of the nozzle but diminishes downstream in the convergent section. At the throat and divergent sections, the wall temperature remains relatively independent of the initial boundary-layer thickness.

VI- The differences in the thermal boundary layer thickness at the inlet are not eradicated by the acceleration imposed by subsonic and throat portions of the nozzle, unlike the momentum boundary layer thickness.

VII- Comparing an 18-inch cooled length to a 0-inch uncooled length, the wall temperature difference at the nozzle entrance is approximately 35%, diminishing to 6% at the throat, and further decreasing towards the nozzle outlet.

Based on the findings, we conclude that the unified approach employed in this study is applicable to problems involving the interaction of high-speed compressible flow and low-speed incompressible flow separated by a solid wall, through the conjugate convection-conduction process.

REFERENCES

1. Marchi, C.H., Laroca, F., Silva, A.F., & Hinckel, J.N., "Numerical solutions of flows in rocket engines with regenerative cooling", *Numer Heat Transfer Part A*, Vol. 45, No.7, 2004, pp. 699–717. https://doi.org/10.1080/10407780490424307

2. Naraghi, M.H., Dunn, S., & Coats, D., "A model for design and analysis of regeneratively cooled rocket engines", Proceedings 40th AIAA/ASME/SAE/ASEE Joint Propulsion Conference, AIAA 2004-3852. https://doi.org/10.2514/6.2004-3852

3. Shope, F.L., "Conjugate conduction-convection heat transfer with a high-speed boundary layer", *J Thermophysics and Heat Transfer*, Vol. 8, No.2, 1994, pp. 275–281. https://doi.org/10.2514/3.534

4. Barbosa, F.I., Zaparoli, E., & Andrade, C.," Unified approach for conjugate heat-transfer analysis of high speed air flow through a water-cooled nozzle", *The Aeronautical Journal*, Vol. 120, No.1224, 2016, pp. 355-373. https://doi.org/10.1017/aer.2015.15

5. Rotta, J. C., "Critical Review of Experimental Heat Transfer Coefficients and Temperature Distributions in Turbulent Boundary Layers at Supersonic and Hypersonic Flow", 1967, NASA-TT-F-10905.

6. Shimura, K., Asako, Y., & Heon, J., "Numerical analysis for supersonic flows in cooled nozzle", *Numer. Heat Transfer Part A*, Vol. 26, No.6, 1994, pp.631-641, https://doi.org/10.1080/10407789408956014

7. Bensayah, K., Hadjadj, A., & Bounif, A, "Heat Transfer in Turbulent Boundary Layers of Conical and Bell-Shaped Rocket Nozzles with Complex Wall Temperature", *Numerical Heat Transfer part A*, Vol. 66, No.3, 2014, pp.289-314. http://dx.doi.org/10.1080/10407782.2013.873283

8. Saeed, R., Mehran, R. Z., & Seyfolah, S., "The effect of nozzle geometry on the flow and heat transfer of pulsed impinging jet on the concave surface", *International Journal of Thermal Sciences*, Vol. 184, 2023, https://doi.org/10.1016/j.ijthermalsci.2022.107925.

9. Wenzel, C., Gibis, T., & Kloker, M., "About the influences of compressibility, heat transfer and pressure gradients in compressible turbulent boundary layers", *Journal of Fluid Mechanics*, 930 A1, 2022, https://doi.org/10.1017/jfm.2021.888

10. Hadjadj, A., Onofri, M., "Nozzle Flow Separation ", *Shock Waves*, Vol. 19, No.3, 2009, pp.163-169. https://link.springer.com/article/10.1007/s00193-009-0209-7

11. Mouronval, A.S., & Hadjadj, A., "Numerical study of the starting process in a supersonic nozzle", *Journal of Propulsion and Power*, Vol. 21, No.2, 2005, pp.374-377.https://doi.org/10.2514/1.6122

12.Hadjadj, A., "Large Eddy Simulation of Shock/Boundary layer interaction", *AIAA journal* Vol. 50, No.12, 2012, pp.2919-2927, https://doi.org/10.2514/1.J051786

13.Ghassan, N., & El-Okda, Y., "Conjugate Effect on the Thermal Characteristics of Air Impinging Jet", *CFD Letters*, Vol. 13, No.10, 2021, pp. 25-35. https://doi.org/10.37934/cfdl.13.10.2535

14.Ghassan, N., El-Okda, Y., Alzaabi, M., Almohsen, H., "Effects of the Conjugate Heat Transfer and Heat Flux Strength on the Thermal Characteristics of Impinging Jets", *CFD Letters*, Vol. 14, No.7, 2022, pp. 18-30. https://doi.org/10.37934/cfdl.14.7.1830

15.Arunkumar, G. L., Shetty, Balachandra P, & Mishra, R. K., "Conjugate heat transfer analysis of a radially cooled nozzle guide vane in an aero gas turbine engine" International Journal of Turbo & Jet-Engines, Vol. 40, No. 1, 2023, pp. 93-100. https://doi.org/10.1515/tjj-2020-0031

16.Hongbing, D., Chao. W., & Gang, W., "Transient conjugate heat transfer in critical flow nozzles", International Journal of Heat and Mass Transfer, Vol. 104, 2017, pp. 930-942. https://doi.org/10.1016/j.ijheatmasstransfer.2016.09.021.

17.Krishna, Z., Cristhian, A., Shoaib, S., John, S., Laith, Z., and Boris, M., "Conjugate Heat Transfer Simulations of a Nozzle Flow over a Film Cooled Plate", Journal of Thermophysics and Heat Transfer, Vol. 37, No.2, 2023, https://doi.org/10.2514/1.T6595

18.Shengxiong, W., Yingkun, L., & Jinsheng X., "Study on conjugate heat transfer characteristics of flexible structure of solid motor nozzle based on multiple working conditions", *Journal of Physics: Conference Series*, Vol. 2472, No. 1, 2023, https://dx.doi.org/10.1088/1742-6596/2472/1/012013.

19.Boldman, D. R., Schmidt, J. F., & Ehlers, R.C., "Effect of Uncooled Inlet Length and Nozzle Convergence Angle on the Turbulent Boundary Layer and Heat Transfer in Conical Nozzles Operating With Air", *Journal of Heat Transfer*, Vol. 89, No.4, 1967, pp.341-350, https://doi.org/10.1115/1.3614395

20.Bartz, D.R.,"A Simple Equation for Rapid Estimation of Rocket Nozzle Convective Heat Transfer Coefficients", *Jet Propulsion*, Vol. 21, 1957, pp. 49-51. https://doi.org/10.2514/8.12572

21.Bartz, D.R., "Turbulent Boundary-Layer Heat Transfer from Rapidly Accelerating Flow of Rocket Combustion Gases and of Heated Air",

Advances in Heat Transfer, Vol. 2, 1965, pp. 1-108. https://doi.org/10.1016/S0065-2717(08)70261-2

22. Bartz, D.R., "An Approximate Solution of Compressible Turbulent Boundary-Layer Development and Convective Heat Transfer in Convergent-Divergent Nozzles", *Trans. ASME*, Vol. 77, No.8, 1955, pp.1235-1245.

23. Back, L.H., Massier, P.F., & Gier, H.L., "Convective heat transfer in a convergent-divergent nozzle", *Int. J. Heat mass Transfer*, Vol. 7, No.5, 1964, pp. 549-568. https://doi.org/10.1016/0017-9310(64)90052-3

24. Back, L.H., Massier, P.F., & Gier, H.L., "Convective heat transfer in a convergent-divergent nozzle", *Technical Report*, *NASA-CR*-57326, 1965, JPL-TR-32-415

25. Gibson, M.M., & Launder, B.E., "Ground effects on pressure fluctuations in the atmospheric boundary layer", *Journal of Fluid Mechanics*, Vol. 86, No.3, 1978, pp.491-511. https://doi.org/10.1017/S0022112078001251

26. Launder, B.E., Reece, G.J., & Rodi, W., " Progress in the development of a Reynolds-stress turbulence closure", *Journal of Fluid Mechanics* Vol. 68, No.3, 1975, pp.537-566. https://doi.org/10.1017/S0022112075001814

27. Launder, Brain E., "Second-moment closure: present... and future?", *International Journal of Heat and Fluid Flow*, Vol. 10, No.4, 1989, pp.282-300. https://doi.org/10.1016/0142-727X(89)90017-9

28. Kumaran, R., Manikanda, P.K., Vivekanand, T., Sundararajan, K., & Kumaresan, Raja. Manohar., "Optimization of Second Throat Ejectors for High Altitude Test Facility", *Journal of Propulsion and Power*, Vol. 25, No.3, 2009, pp.697–706. https://doi.org/10.2514/1.39219

29. Kumaran R., Manikanda, T., & Sundararajan, Raja. Manohar., "Simulation of High Altitude Tests for Large Area Ratio Rocket Motors", *AIAA Journal*, Vol. 51, No.2, 2013, pp. 433–443. https://doi.org/10.2514/1.J051842

30. Rajagopal, Manikanda., "Numerical Modeling of Regenerative Cooling System for Large Expansion Ratio Rocket Engines", *J. Thermal Sci. Eng. Appl*, Vol. 7, No.1, 2015, 011012. https://doi.org/10.1115/1.4028979

31. Gordon, S., & Mcbride, B.J., "Chemical Equilibrium with Applications (CEA). *NASA Lewis Research Center (now NASA Glenn Research Center)*, USA. In: online program CEARUN, https://cearun.grc.nasa.gov/

32. Smits, J.A., & Dussauge, J.P., "Turbulent Shear Layers in Supersonic Flow" Springer; 2nd edition (May 11, 2006) ISBN-13: 978-0387261409

33. Debiève, J.F., Dupont, P., Smith, D.R., & Smits, J.A., "Supersonic Turbulent Boundary Layer Subjected to Step Changes in Wall Temperature", *AIAA Journal*, Vol. 35, No.1, 1997, pp. 51-57. https://doi.org/10.2514/2.86.